UC Riverside
UC Riverside Previously Published Works

Title
Real-time transposable element activity in individual live cells

Permalink
https://escholarship.org/uc/item/3bf8w631

Journal
Proceedings of the National Academy of Sciences of the United States of America, 113(26)

ISSN
0027-8424

Authors
Kim, Neil H
Lee, Gloria
Sherer, Nicholas A
et al.

Publication Date
2016-06-28

DOI
10.1073/pnas.1601833113

Peer reviewed

Real-time transposable element activity in individual live cells

Neil H. Kim (김현일)[a,b], Gloria Lee[a,b], Nicholas A. Sherer[a,b], K. Michael Martini[a,b], Nigel Goldenfeld[a,b,c,d,1], and Thomas E. Kuhlman[a,b,e,1]

[a]Department of Physics, University of Illinois at Urbana–Champaign, Urbana, IL 61801; [b]Center for the Physics of Living Cells, University of Illinois at Urbana–Champaign, Urbana, IL 61801; [c]Institute for Universal Biology NASA Astrobiology Institute, University of Illinois at Urbana–Champaign, Urbana, IL 61801; [d]Carl R. Woese Institute for Genomic Biology, University of Illinois at Urbana–Champaign, Urbana, IL 61801; and [e]Center for Biophysics and Quantitative Biology, University of Illinois at Urbana–Champaign, Urbana, IL 61801

The excision and reintegration of transposable elements (TEs) restructure their host genomes, generating cellular diversity involved in evolution, development, and the etiology of human diseases. Our current knowledge of TE behavior primarily results from bulk techniques that generate time and cell ensemble averages, but cannot capture cell-to-cell variation or local environmental and temporal variability. We have developed an experimental system based on the bacterial TE IS608 that uses fluorescent reporters to directly observe single TE excision events in individual cells in real time. We find that TE activity depends upon the TE's orientation in the genome and the amount of transposase protein in the cell. We also find that TE activity is highly variable throughout the lifetime of the cell. Upon entering stationary phase, TE activity increases in cells hereditarily predisposed to TE activity. These direct observations demonstrate that real-time live-cell imaging of evolution at the molecular and individual event level is a powerful tool for the exploration of genome plasticity in stressed cells.

transposable elements | evolution | quantitative biology

A transposable element (TE) is a mobile genetic element that propagates within its host genome by self-catalyzed copying or excision followed by genomic reintegration (1). TEs exist in all domains of life, and the activity of TEs necessarily generates mutations in the host genome. Consequently, TEs are major contributors to disease (2–8), development (9, 10), and evolution (11, 12); they are also used as molecular tools in synthetic biology and bioengineering (13).

Despite their ubiquity and importance, surprisingly little is known about the behavior and dynamics of TE activity in living cells. TE propagation rates can be inferred from comparative phylogenetic analyses of related organisms (14–20) or endpoint analyses of TE abundance within populations (11, 21–23). By making assumptions about the mechanisms of TE proliferation, models can be constructed to describe the distribution of TEs within genomes over evolutionary time scales, and sequenced genomes can be analyzed and fit to TE proliferation models to infer phylogeny of TE copies and estimate their rates of propagation (24). However, most sequencing techniques require bulk sampling of cells to provide genetic material, and sequencing is therefore generally an average over many cells. As a result, without extremely deep or single-cell sequencing techniques, most current methods are sufficient to detect only those TE events that have occurred in the germ line and therefore appear in every somatic cell in the body (25).

TE rates can also be estimated by measuring relative abundances in populations that have been allowed to mutate over laboratory time scales. One of the first examples of this approach was that by Paquin and Williamson (23) to study the effects of temperature on the rate of integration of Ty retrotransposons in *Saccharomyces cerevisiae* after growth for 6–8 generations, resulting in yeast resistant to the antibiotic antimycin A; they estimated a rate of transposition of 10^{-7}–10^{-10} insertions into a

particular region of the yeast genome per cell per generation. As another example, sequencing of *Escherichia coli* at intervals in Lenski's long-term evolution experiments also provided a means to estimate transposition frequency, which they estimate to be on the order of 10^{-6} per cell per hour (11). However, such measurements yield information on only the relative abundance of extant TE-affected cells in the population, and dynamic rates must again be inferred through models of population growth that may or may not be accurate.

The limitations described above mean that there is a dearth of information regarding TE behavior in individual living cells in vivo and the effects of TE activity on those cells. Additionally, estimation of transposition frequency from either phylogenetic comparisons or population endpoint analyses both suffer from the same serious and fundamental limitation: they are only able to detect those events that have not gone to extinction in the population, and therefore these methods almost certainly underestimate the actual rates of transposition. An analogous situation previously existed in the case of the dynamics of horizontal gene transfer: phylogenetically inferred rates of horizontal gene transfer are typically 1 per 100,000 y, whereas direct visual observation in experiments (26) has shown that the actual transfer rate is many orders of magnitude faster, about one per generation time.

To quantitatively study the dynamics of TE activity and its controlling factors in real time and in individual cells, we have constructed a TE system based on the bacterial TE IS608 in *E. coli*. IS608 is a representative of the IS200/IS605 family of

Significance

We have followed in real time how transposable elements, or "jumping genes," move around in the genome of a living organism. Using a simple plasmid-borne transposable element, we have measured directly and precisely how frequently cells are affected by transposable elements and what factors contribute to their activity. We find the activity of this simple transposable element to be surprisingly rich, depending upon the host cell's growth and environmental factors. Application of this system to more complex natural transposable elements will enable a quantitative understanding of these fundamental dynamical elements of all genomes, informing our understanding of genome plasticity and the mutations that can give rise to disease and drive evolution.

transposable elements, which all transpose through similar mechanisms. The IS200/IS605 family is widely distributed, with 153 distinct members spread over 45 genera and 61 species of eubacteria and archaea (27). Transposition occurs by exact excision from a single DNA strand (21, 28–32). Imperfect palindromic sequences flanking the ends of the TE form unique structures that are recognized by transposase protein TnpA, which can act as a homodimer to excise the TE. The excised TE–TnpA complex can locate and integrate the TE adjacent to a short, specific sequence (TTAC). Our construct exploits the structure and regulation of the TE to allow the direct detection and quantification of TE activity in live cells using a suite of novel fluorescent reporters.

Results

TE Observation System. A diagram illustrating the TE system is shown in Fig. 1A. The TE is composed of the transposase coding sequence, tnpA, flanked by a left end imperfect palindromic sequence (LE IP) and right end imperfect palindromic sequence (RE IP), which are the recognition and cleavage sites for TnpA. tnpA is expressed using the promoter P_{LTetO1}, which is repressed by tet repressor. P_{LTetO1} is derived from the E. coli transposable element Tn10 and titratable over a ~100× range with

Fig. 1. Design and validation of the TE system. (A) The promoter for mCerulean3 is interrupted by the transposable element, the ends of which are demarcated by left end and right end imperfect palindromic sequences (LE IP and RE IP). The transposase, tnpA (gray), is expressed from the promoter P_{LtetO1}, which is inducible with aTc. The sequences of the promoter/TE junction and −10 and −35 sequences (red boxes) are shown below the diagram, and the sites cleaved by transposase are indicated by arrows. (B) Upon excision, the promoter for mCerulean3 is reconstituted and the cell fluoresces blue. The sequence of the reconstituted promoter is shown below the diagram. A primer designed to bind to the unique sequence formed after promoter reconstitution (blue arrow) was used to verify excision by PCR, generating an 858-bp amplicon. (C) PCR amplification using these primers only generates the 858-bp product upon induction, thus verifying excision. (D–F) Colony morphology after growth on agarose pads. Uninduced TE-carrying cells (D) and wild-type cells exposed to 20 ng/mL aTc (F) show homogeneous, low blue autofluorescence. Conversely, TE-carrying cells induced with 20 ng/mL aTc (E) show bright, inhomogeneous blue fluorescence. The brightness scale for all three images is identical. The borders of the colonies are outlined in white.
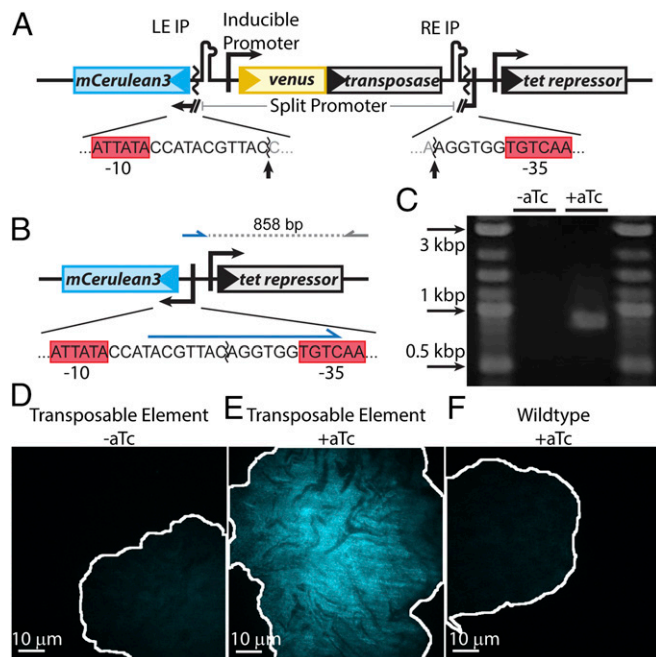
anhydrotetracycline (aTc) (33). The use of this inducible promoter allows for simple and precise control of TnpA levels within individual cells. The TE splits the −10 and −35 sequences of a strong constitutive P_{lacIQ1} promoter (34) for the expression of the blue reporter mCerulean3 (35). As shown in Fig. 1B, when transposase production is induced, the TE can be excised, leading to reconstitution of the promoter. The resulting cell expresses mCerulean and fluoresces blue, indicating that an excision event has occurred. The N terminus of TnpA is translationally fused to the bright yellow reporter Venus (36), and the cells constitutively express the red reporter mCherry (37) to aid in image segmentation. Measurements of blue, yellow, and red fluorescence of controls demonstrate no cross-talk in our optical setup (Fig. S1). The TE is hosted in the low copy number plasmid pJK14 with a pSC101 replication origin (38).

Verification of TE Observation System. We first confirmed that the TE excises upon induction of transposase production. PCR was performed using primers that bind to the unique sequence formed upon excision, and cells containing the TE and induced with aTc yielded product with amplicons of the expected length (Fig. 1C). We next verified that transposase induction results in expected patterns of fluorescence corresponding to TE excision. When TE-carrying E. coli are grown on agarose pads with aTc, the resulting microcolonies exhibit spatially distinct bright and dark regions of blue fluorescence (Fig. 1E). This observation is expected from plasmids expressing blue fluorescent proteins after some have undergone TE excision, followed by plasmid inheritance by daughter cells, and will be discussed in more detail below. Conversely, microcolonies arising from an identically treated wild-type negative control strain carrying no plasmids and an uninduced TE-carrying strain are fluorescently dim and homogeneous (Fig. 1 D and F).

Quantification of Excision Response to Transposase Concentration. It is reasonable to expect that TE excision probabilities may be a function of intracellular transposase concentration. This straightforward expectation has proven difficult to experimentally characterize, however, due to low-throughput sampling of transposase concentration provided by population sequencing and other bulk techniques (39). By comparing the intensity of yellow fluorescence and blue fluorescence of single cells titrated over a wide range of transposase inducer, we were able to determine the in vivo excision response function to transposase concentration.
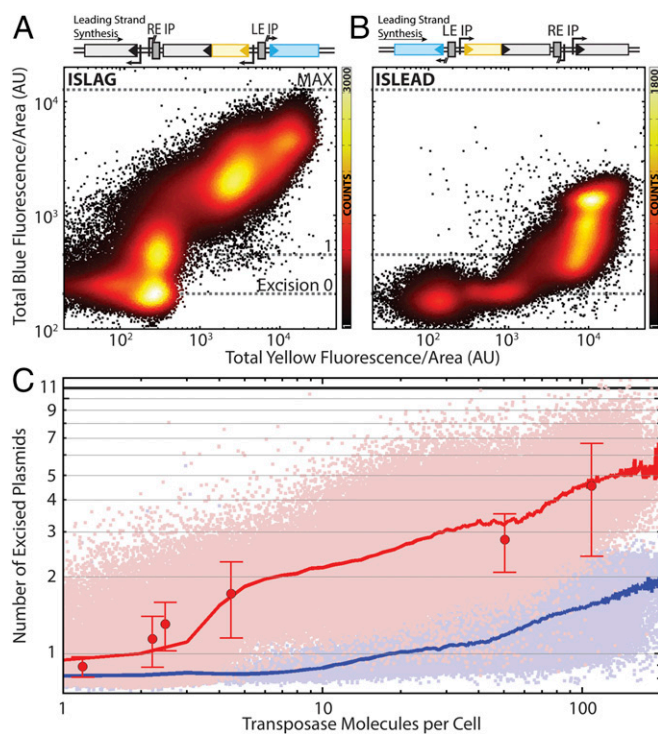
TE-carrying cells were grown in medium titrated with aTc concentrations ranging from 0 to 1,000 ng/mL. We constructed two versions of the TE, one with the imperfect palindromic sequences encoded in the leading strand (ISLEAD) and the other with the imperfect palindromic sequences encoded in the lagging strand (ISLAG). After ~12–13 doublings, each sample was imaged using highly inclined and laminated optical sheet (HILO) laser illumination (40, 41). Fig. 2 shows scatterplots of blue fluorescence vs. yellow fluorescence for individual cells carrying ISLAG (Fig. 2A) or ISLEAD (Fig. 2B). The response functions for ISLAG and ISLEAD are qualitatively different, with the ISLAG construct responding more quickly at low aTc concentrations and the ISLEAD construct responding at higher aTc concentrations. The transposase promoter's nonlinear response to aTc (Fig. S2) results in nonuniform count densities along the x axis. To determine if translational fusion of Venus to TnpA affected transposase expression, a version of ISLAG without Venus fused to TnpA was also assayed. The construct showed quantitatively identical behavior (Fig. S3).

We next quantified the number of transposase molecules and induced excisions based on the intensity of yellow and blue fluorescence. The result is shown in Fig. 2C, with mean response functions of ISLAG and ISLEAD shown as red and blue lines, respectively.

Fig. 2. TE excision response function. Scatterplots of blue vs. yellow total cellular fluorescence divided by cell area for TE encoded in the (*A*) lagging (N_{cells} = 192,965) and (*B*) leading (N_{cells} = 101,709) strand of the host plasmid. Colors indicate number of counts in each bin of a 500 × 500 grid covering the data. (*C*) The same data as in *A* and *B* with absolute axes. The *y* axis is expressed in terms of the absolute number of excised plasmids, and the *x* axis is scaled to absolute number of transposase molecules per cell. Light-red and -blue points are lagging and leading strand data from *A* and *B*, respectively. Red and blue lines are excised plasmid number averaged according to transposase molecules binned as integer quantities. Large red points indicate the number of excised plasmids as measured by qPCR; error bars are the SEM of three experimental replicates. See also Fig. S3.

To estimate the absolute number of transposase molecules induced, the bleaching kinetics of Venus-TnpA were analyzed based on a theoretical technique developed by Nayak and Rutenberg (42), discussed in detail in *SI Experimental Procedures*. ISLAG cells were grown as described above, and transposase expression was induced with 100 ng/mL aTc. At OD_{600} = 1.0, cells were mounted on a slide and their bleaching kinetics recorded via fluorescence microscopy. By recognizing fluctuations from the mean bleaching kinetics of Venus-TnpA as binomial noise, the bleaching curves of individual cells can be analyzed to estimate the constant of proportionality, ν, relating fluorescent intensity to the number of fluorescent molecules. We find $\nu = 130 \pm 10$ from the analysis of 419 cells (Fig. S4 and *SI Experimental Procedures*).

To determine how blue fluorescence intensity represents excision numbers, we measured the mean blue fluorescence of a wild-type negative control carrying no plasmids, as well as a control in which every plasmid expresses mCerulean. Their average intensities correspond to the mean fluorescence of cells with no excisions and cells with all TEs excised, respectively (Fig. 2 *A* and *B*, excision 0 and MAX). From the excision response curve, one can see a clear distinction in the blue fluorescence of cells with no excisions and those with one TE excision (Fig. 2 *A* and *B*, line 1). And our simulation shows that blue fluorescence intensity is expected to be proportional to the number of excised plasmids (Fig. S5). Therefore, by using quantitative PCR (qPCR) to determine the average plasmid copy number in each cell, the *y*

axis can be scaled in terms of the average absolute number of excised plasmids.

To further verify that fluorescence accurately represents TE excision number, qPCR measurements of lagging strand TE excisions over a range of transposase inducer concentrations were performed (Fig. 2*C*, red points) using primers that produce an amplicon only when excised plasmid is present. At the highest transposase numbers we achieve, ~50% of the average total 11–12 plasmids per cell are excised (Fig. S6).

Observing Real-Time Kinetics. By growing TE-carrying cells on agarose pads including aTc under the microscope, TE excision events can be detected in real time and their rates and statistics determined through direct observation. We find that TE activity changes as cells undergo different phases of growth, and that TE activity correlates to where cells are located within a colony.

Excision Rates Depend on Growth State of Cells. At high-inducer concentrations (>10 ng/mL aTc; Fig. 1*E*), a large fraction of cells immediately experiences TE events and fluoresces blue. At low-inducer and transposase concentrations (<10 ng/mL aTc), we can observe individual excision events as bright flashes of blue fluorescence whose rate depends upon the growth state of the cells. As cells initially adapt to the pad, some fraction rapidly fluoresce blue, indicating TE excision. Once cells enter exponential growth, the frequency of cells becoming fluorescent drops to nearly zero; the fluorescence patterns observed in mature microcolonies at low inducer concentrations (Fig. 3*A*) arise primarily from inheritance of the initial excision events. However, upon entering final growth arrest, some cells begin to emit bright blue fluorescence (Fig. 3 *A*–*C* and Movie S1) accompanied by an increase in yellow fluorescence (Fig. 3*D* and Movie S2). The polar localization of Venus-TnpA seen in Movie S2 is a known consequence of nucleoid condensation and volume exclusion in stationary phase (41, 43). Note in Fig. 3*D* that the excision event (blue line) is preceded by a weak increase in transposase levels (yellow fluorescence), indicating transposase-induced excision. Control strains, including a wild-type TE-less strain exposed to aTc, TE-carrying cells not exposed to aTc, and cells constitutively expressing mCerulean3, do not show similar bursts of fluorescence (Movie S3).

Excision Event Rate Is Constant Once Initiated. Automated identification of TE fluorescence events within each colony (Movie S4) reveals that events begin occurring with the onset of growth arrest and continue at a rate that remains approximately constant for >35 h (Fig. 3*E*). The average event rate for this experiment, consisting of 12 colonies and ~5,000 cells, was $6.3 \pm 2.6 \times 10^{-3}$ events per cell per hour. The temporal statistics are consistent with events, once initiated upon growth arrest, occurring randomly in time as described by Poisson statistics (Fig. 3*F*).

Excision Events Are Spatially Correlated. Events are not uniformly random in space and are instead spatially clustered and dependent upon the location in the colony. Events are less common within ~3 μm (~5 cell widths) of the colony edge compared with the center (Fig. 3*G* and Fig. S7). The mean pair radial correlation, $g(r)$, also shows that events are clustered together (Fig. 3*H*, blue line, and *SI Experimental Procedures*).

We performed simulations of *E. coli* growth into microcolonies combined with random distributions of TE events to determine the expected properties of $g(r)$ arising from randomly spaced TE events within an *E. coli* colony. Simulations were used to generate 200 different microcolony morphologies, each starting from a single cell and ending upon reaching a size representative of those we observe in our experiments (~300 cells with a diameter of ~15–16 μm). After growth arrest, 15% of the cells within each colony morphology were chosen at random to
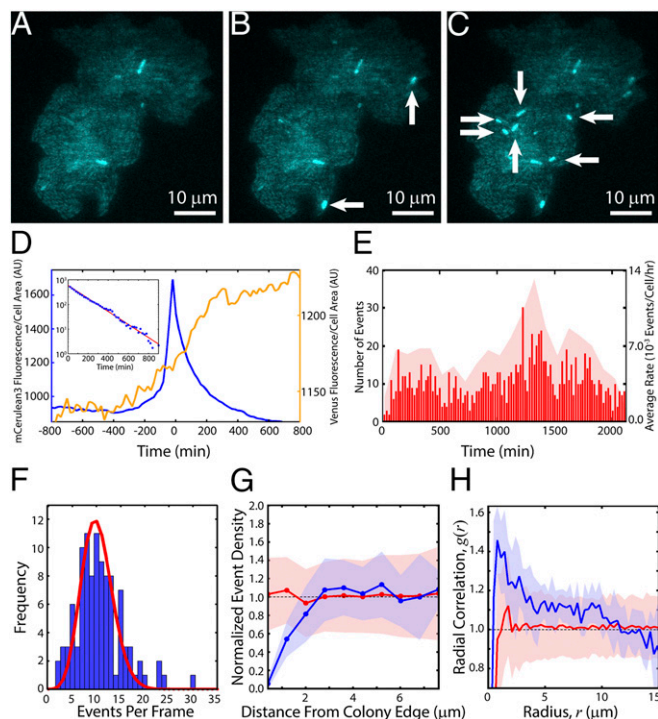
Fig. 3. Real-time TE kinetics. Colony induced with 5 ng/mL aTc undergoing excision events at (*A*) *t* = 0 (time of first detected events, after ~10 h of growth), (*B*) *t* = 40 min, and (*C*) *t* = 60 min. New events are indicated by white arrows. (*D*) mCerulean3 and Venus-TnpA traces for an average event. TE events were aligned with peak mCerulean3 intensity at *t* = 0. Shown is the mean mCerulean3 (blue, left *y* axis) and Venus-TnpA (yellow, right *y* axis) fluorescence per cell area as a function of time averaged over 773 events. (*Inset*) Decay of mCerulean3 fluorescence as a function of time. Red line is a fit to an exponential $f(t) = A \exp(-bt)$, with $A = 589$ and $b = -0.006$ min^{-1}, consistent with photobleaching. (*E*) Raster plot of all events in a single experiment (red lines, left *y* axis) with *t* = 0; $N_{colonies} = 12$, $N_{cells} = 4,858$, $N_{events} = 1,114$. The average rate was $6.3 \pm 2.6 \times 10^{-3}$ events per cell per hour. Red shaded region shows the average rates during 100-min intervals (right *y* axis). (*F*) Blue bars: frequency of the number of events per frame. Red line: distribution of events per frame expected from a Poisson process with an average rate of 6.3×10^{-3} events per cell per hour. (*G*) Within each colony, we determine the event densities within annuli of width 0.8 μm at various distances from the colony edge (Fig. S7). We then took an ensemble average over all colonies, where the density in each colony is normalized by the mean event density over the entire colony. Blue line: mean normalized density of events in 0.8-μm-wide annuli vs. the distance of the center of each annulus from the colony edge; shaded blue region is the SD. Red line: mean normalized density obtained from simulations of randomly spaced events; shaded red region is the SD. (*H*) Blue line: mean pair correlation function, *g*(*r*), of events; shaded blue region is the SD. Red line: *g*(*r*) of randomly spaced events obtained from simulations; shaded red region is the SD.

undergo TE events, a rate representative of the average final number of affected cells in each colony we observe experimentally. By comparing *g*(*r*) between experiment and simulation, we find that the density of events in adjacent cells in our experiment is ~1.4× greater than expected compared with the simulation of events randomly distributed in space (Fig. 3*H*, red line, Movie S5, and *SI Experimental Procedures*).

Distribution of Rates Is Consistent with Additional Control by a Heritable Luria–Delbrück Process. The nonuniform event distributions in space suggest that local environmental differences and/ or a hereditary process are influencing TE activity. A distribution of event rates determined from 984 colonies is shown in Fig. 4*A*, with a mean rate of $11.8 \pm 12 \times 10^{-3}$ events per cell per hour per colony. (This is compatible with overall number of events per frame following a Poisson distribution; Fig. 3*F* and *SI Experimental*

Procedures.) To explain the distribution of colony event rates shown in Fig. 4*A*, we simulated a two-step process (44, 45). First, in a Luria–Delbrück process after cells are placed on the pad, some stochastic heritable change can occur with constant probability during exponential growth that predisposes cells to TE activity (Fig. 4*B*). In the simulation, 10,000 cell colonies were simulated to grow until they reached colony sizes drawn from the colony size distribution observed in the experiment. While in growth, a heritable change occurs in a daughter cell after each division with probability p_h. From the affected cell, the change is inherited by all of its descendants. In growth arrest, any cell that has inherited the change can then experience a TE excision with probability p_e. A good fit of event densities was found (Fig. 4*A*, red line) by searching through the two parameters with a goodness criterion (*SI Experimental Procedures*). This analysis and the quality of the fit strongly suggest that the average event rate in each colony is determined by some stochastic, heritable change occurring in the lineage—for example, expression bursts, or lack thereof, of long-lived tet repressor protein.

Discussion

Our goal is to begin the quantitative understanding of how TEs fundamentally function and behave in single live cells before understanding more complex systems. Placing the TE under an inducible promoter allows us to precisely control and determine how TE excisions respond to transposase concentration. Examining the bleaching kinetics of Venus-TnpA allows us to estimate absolute numbers of transposase proteins within individual cells, which improves upon previous studies that could only infer mean TnpA levels from the applied inducer concentrations. Though we use a synthetic *tet* promoter derived from an *E. coli* TE to express TnpA instead of the natural *tnpA* promoter, the transposase levels in any wild-type system will still sample from the same response function. That even this simple system exhibits complex dynamic behavior illustrates the necessity of using real-time single-cell measurements rather than population and time-averaged estimates of TE kinetics, a parallel to the way in which real-time single-molecule measurements have revolutionized our understanding of the rich dynamics hidden by population-averaged ensemble measurements (46). This quantification of genome plasticity in real time permits the development of a precise narrative of the role of TE activity in evolution and even epidemiology.

The single-cell response curves shown in Fig. 2 are consistent with existing molecular models of how TnpA binds to and excises
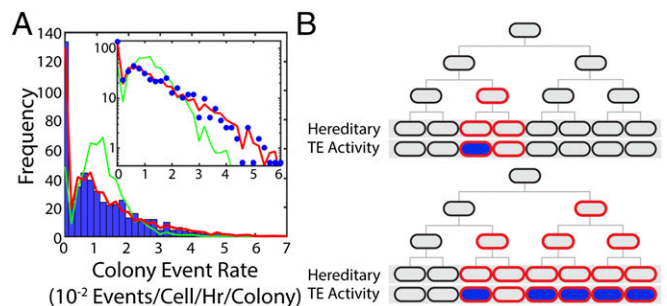
Fig. 4. Event rates are determined by a stochastic heritable change. (*A*) Blue bars: distribution of average event rates for individual colonies with [aTc] = 5 ng/mL; $N_{colonies} = 984$. The mean rate of this distribution is $11.8 \pm 12 \times 10^{-3}$ events per cell per hour per colony. Red line: result of a two-step process simulated using the experimental distribution of colony sizes. Green line: result of a Poisson process with the mean rate of the experimental distribution. (*Inset*) Same data with logarithmic *y* axis. (*B*) Cartoon picture illustrating the Luria–Delbrück process used in our simulation where some fraction of cells inherit a trait that predisposes them to TE activity (red outline), and of those cells some fraction fluoresce blue (blue fill), indicating TE activity.

the TE from the host DNA molecule (21). The response function displays qualitatively distinct behavior in the leading vs. lagging strand. Because the lagging strand of DNA is discontinuously replicated, the lagging strand leaves single-stranded DNA exposed while synthesis of Okazaki fragments is completed. Hence, it is more energetically favorable for the folded imperfect palindromic sequences recognized by TnpA to form in the lagging strand than the leading strand, where the energetically favored state is canonically base-paired double-stranded DNA (21). Consequently, the TE in the lagging strand is extremely sensitive to TnpA, with the first excisions occurring in the presence of only 1–2 TnpA dimers. Conversely, ~10× higher TnpA numbers are required to initiate excision from the leading strand.

Real-time imaging allows us to track how TE activity varies from one cell to another within different colonies over time. We found that upon growth arrest, excision events are distributed nonuniformly within each colony. This nonuniformity can be described with a Luria–Delbrück process, suggesting that some stochastic, heritable trait predisposes a fraction of cells to TE activity. Additionally, the relative lack of excision activities observed near the edges of colonies may arise from local environmental variation, such as nutrient availability, between the edge and center of a colony. Together, these results demonstrate that the rate of TE excision is highly dynamic and depends upon the amount of transposase in the cell, the TE's orientation within the genome, the growth state and life history of the host cell, and the cell's local environment.

Though here we focus solely on excision, we note that because excision of a TE is required before reintegration, it is likely that integrations and the mutations they generate will occur with a rate that is dependent upon the excision rate measured here. Previous studies detecting transposition in vivo using time-averaged population-level methods have estimated the convolved transposition rates, i.e., the combined rates of both excision and integration, as a result of experimental or conceptual limitations in separating the two processes. Mating-out assays, for example, detect TE integration only into a conjugative plasmid which is then transferred to a virgin recipient strain for detection (47). These methods therefore only measure the combined rate of excision, integration to the plasmid, and conjugation of the plasmid merged together. From a mechanistic standpoint, excision and integration are two separate processes that should be understood independently. It is necessary to know excision rates independently of reintegration to understand how stable transposable elements are in the genome. Furthermore, an excision itself is a mutation carrying biological significance. Any genes carried by the TE will be lost, and if the TE has silenced a gene by interrupting it, then excision may restore its function.

One of the primary results of this work is the observed heterogeneity of TE activity rates in both space and time. In a sense, this is surprising; the design of the synthetic TE used here is extremely simple, and yet it shows complex spatial and temporal dynamics. Furthermore, since the fundamental experiments of Luria and Delbrück, the uniform randomness and homogeneity of mutation rates is frequently taken as a starting point for descriptions and models of mutation and evolution. However, as shown in Fig. 2, the activity of the TE is a direct function of the intracellular numbers of TnpA protein. Because it is well known that intracellular protein levels are strongly influenced by the cellular growth state (48), cell-to-cell and temporal heterogeneity in intracellular TnpA amounts and the resulting TE activity levels should perhaps be anticipated. Similar arguments can readily be made about any other mutational process that relies upon the activity of an expressed protein for its generation or repair—for example, the repair of nascent point mutations by the proteinaceous mismatch repair system (49).

It is difficult to draw direct and meaningful comparisons between our measurements of TE excision rates and previous measurements. Previously measured transposition rates (i.e., excision followed by reintegration) are on the order of 10^{-6}–10^{-10} transpositions per cell per doubling (23), or transpositions per cell per hour (11), whereas the excision rates that we measure are several orders of magnitude greater. A variety of hypotheses can be proposed to reconcile these results. For example, it is possible that reintegration is extremely inefficient and only successful for a small fraction of excisions. However, we have observed that expression levels of Venus-TnpA in these and other longer time-scale measurements do not decrease over time, which suggests this is not the case. It is also possible that previous experiments underestimate TE activity rates as a result of insufficiently deep sampling, or the deleterious physiological effects of the TE leading to extinction of affected cells within the population. The reason for this discrepancy remains unclear and is a subject for future work.

Experimental Procedures

Detailed procedures for all constructs and experiments can be found in *SI Experimental Procedures*.

Strains. Experiments were performed using *E. coli* K-12 MG1655 Δ*lac* (41, 43, 50, 51) expressing the red fluorescent protein mCherry (37) from a strong P_{lacIQ} constitutive promoter integrated into the *n*th chromosomal locus located near the replication terminus (41, 50). Molecular cloning and plasmid manipulations were performed using DH5α as a host strain.

Plasmid Construction. The low copy number plasmid pJK14 (38) was used to host the TE in all experiments. pJK14 has a pSC101 replication origin and is replicated unidirectionally, i.e., there is a well-defined leading and lagging strand. Plasmid copy number is tightly controlled through the positive feedback of the plasmid-encoded protein RepA (52). Additionally, pJK14 is actively segregated to daughter cells through the pSC101 *par* system (53).

Plasmid pJK14-ISLEAD was designed using Vector NTI software (Life Technologies) and synthesized de novo by GENEWIZ Gene Synthesis Services (GENEWIZ, Inc.). Variants including pJK14-ISLAG were generated through standard molecular cloning techniques, described in detail in *SI Experimental Procedures*.

Microscopy and Image Analysis. To measure the TE excision response functions in Fig. 2, cells carrying the indicated version of the TE were grown overnight in Lysogeny broth (LB). An appropriate volume of the culture was added to M63 minimal medium + 0.5% (vol/vol) glycerol and 25 μg/mL kanamycin to yield an initial $OD_{600} = 0.0002$. To these tubes, varying concentrations of aTc were added to titrate cells with inducer. These tubes were grown at 37 °C with vigorous shaking until OD_{600} ~1.5. At this point, samples were taken from each tube for imaging.

A Nikon Eclipse Ti-E fully automated inverted microscope was used for imaging. To generate the transposase response curves, cells were placed on a glass slide and squeezed with a coverslip to ensure that as many as possible were lying flat in the focal plane. For each slide, we took 200 images. Each image contains information captured from three fluorescent channels: mCherry (red), Venus (yellow), and mCerulean3 (blue), in that order. Fluorescent excitation was performed using HILO laser illumination (40) with 561nm (mCherry excitation; cell area), 514 nm (Venus excitation, Venus-TnpA levels), and 457 nm (mCerulean3 excitation, excision reporting) in that order. The 561-nm excitation was provided by a 50-mW Sapphire laser (Coherent); both 514-nm and 457-nm excitation were provided by a 40-mW Argon laser (CVI Melles Griot). Filter sets used were HQ560/55× ET645/75m (mCherry), ZET514/10× ET535/30m (Venus), and Z457/10× ET485/30m (mCerulean3). We observed no anomalous aggregation of mCherry, Venus-TnpA, or mCerulean3 (40), and the maturation times of Venus and mCerulean3 are both less than 10 min at 37 °C (36, 54, 55).

To directly quantify TE excision rates shown in Fig. 3, 5 μL of a MG1655 Δ*lac n*th <P_{lacIQ}-*mCherry*> pJK14-ISLAG culture in exponential growth at $OD_{600} = 0.05$ was placed on an M63 glycerol medium agarose pad containing the appropriate antibiotics, that was cast on a glass slide. The sample was covered with a glass coverslip and allowed to settle for 20 min before being sealed with epoxy glue to prevent drying.

For imaging, the slide was placed onto a Nikon Eclipse Ti-E inverted microscope. The sample was maintained at 37 °C in a temperature-controlled environmental chamber. Images consisting of 40–80 adjacent fields of view were taken every 20 min in each of three fluorescent channels: mCherry, Venus, and mCerulean3.

Image analysis was performed using custom image segmentation and analysis algorithms implemented in MATLAB (MathWorks). Cell identification and image segmentation was performed using the red channel, where all cells are homogeneously fluorescent with high signal-to-background noise ratio due to constitutive mCherry expression.

Quantitative PCR. Average plasmid copy numbers per cell for uninduced pJK14-ISLAG, induced pJK14-ISLAG, and the control plasmid pJK14-mCerulean3 were determined by qPCR with a Bio-Rad CFX96 Touch Real-Time PCR thermal cycler using SsoAdvanced Universal SYBR Green Supermix (Bio-Rad). Cells were grown as described above for imaging. Once the appropriate density of each strain was achieved, samples were taken for plating to determine the number of cells added to each PCR.

qPCR was performed on each sample in triplicate. In the same plate, a standard curve was generated using purified pJK14-ISLAG plasmid with known molarity

determined by measurement of absorbance at 260 nm in a NanoDrop 2000c spectrophotometer (Thermo Scientific). See *SI Experimental Procedures* for details.

To determine relative number of TE excisions per cell (Fig. 2C, large red points), qPCR was performed as described above on cells induced with different concentrations of aTc. See *SI Experimental Procedures* for details.

1. McClintock B (1950) The origin and behavior of mutable loci in maize. *Proc Natl Acad Sci USA* 36(6):344–355.
2. Belancio VP, Deininger PL, Roy-Engel AM (2009) LINE dancing in the human genome: Transposable elements and disease. *Genome Med* 1(10):97.
3. Bodega B, Orlando V (2014) Repetitive elements dynamics in cell identity programming, maintenance and disease. *Curr Opin Cell Biol* 31:67–73.
4. Callinan PA, Batzer MA (2006) Retrotransposable elements and human disease. *Genome Dyn* 1:104–115.
5. Chen JM, Stenson PD, Cooper DN, Férec C (2005) A systematic analysis of LINE-1 endonuclease-dependent retrotranspositional events causing human genetic disease. *Hum Genet* 117(5):411–427.
6. Deininger PL, Batzer MA (1999) Alu repeats and human disease. *Mol Genet Metab* 67(3):183–193.
7. Kazazian HH, Jr, et al. (1988) Haemophilia A resulting from de novo insertion of L1 sequences represents a novel mechanism for mutation in man. *Nature* 332(6160):164–166.
8. O'Donnell KA, Burns KH (2010) Mobilizing diversity: Transposable element insertions in genetic variation and disease. *Mob DNA* 1(1):21.
9. Coufal NG, et al. (2009) L1 retrotransposition in human neural progenitor cells. *Nature* 460(7259):1127–1131.
10. Kano H, et al. (2009) L1 retrotransposition occurs mainly in embryogenesis and creates somatic mosaicism. *Genes Dev* 23(11):1303–1312.
11. Schneider D, Lenski RE (2004) Dynamics of insertion sequence elements during experimental evolution of bacteria. *Res Microbiol* 155(5):319–327.
12. Chao L, Vargas C, Spear BB, Cox EC (1983) Transposable elements as mutator genes in evolution. *Nature* 303(5918):633–635.
13. Reznikoff WS (2009) Transposable elements. *Encyclopedia of Microbiology*, ed Schaechter M (Academic, Oxford), 3rd Ed, pp 680–689.
14. Kohl S, Bock R (2009) Transposition of a bacterial insertion sequence in chloroplasts. *Plant J* 58(3):423–436.
15. Parisod C, et al. (2012) Differential dynamics of transposable elements during long-term diploidization of Nicotiana section Repandae (Solanaceae) allopolyploid genomes. *PLoS One* 7(11):e50352.
16. Petrov DA, Fiston-Lavier AS, Lipatov M, Lenkov K, González J (2011) Population genomics of transposable elements in *Drosophila melanogaster*. *Mol Biol Evol* 28(5):1633–1644.
17. Schaack S, Pritham EJ, Wolf A, Lynch M (2010) DNA transposon dynamics in populations of *Daphnia pulex* with and without sex. *Proc R Soc B Biol Sci* 277(1692):2381–2387.
18. Shen JJ, Dushoff J, Bewick AJ, Chain FJ, Evans BJ (2013) Genomic dynamics of transposable elements in the western clawed frog (*Silurana tropicalis*). *Genome Biol Evol* 5(5):998–1009.
19. Venner S, Feschotte C, Biémont C (2009) Dynamics of transposable elements: Towards a community ecology of the genome. *Trends Genet* 25(7):317–323.
20. Wright SI, Le QH, Schoen DJ, Bureau TE (2001) Population dynamics of an Ac-like transposable element in self- and cross-pollinating *Arabidopsis*. *Genetics* 158(3):1279–1288.
21. Ton-Hoang B, et al. (2010) Single-stranded DNA transposition is coupled to host replication. *Cell* 142(3):398–408.
22. Papadopoulos D, et al. (1999) Genomic evolution during a 10,000-generation experiment with bacteria. *Proc Natl Acad Sci USA* 96(7):3807–3812.
23. Paquin CE, Williamson VM (1984) Temperature effects on the rate of ty transposition. *Science* 226(4670):53–55.
24. Le Rouzic A, Payen T, Hua-Van A (2013) Reconstructing the evolutionary history of transposable elements. *Genome Biol Evol* 5(1):77–86.
25. Goodier JL (2014) Retrotransposition in tumors and brains. *Mob DNA* 5:11.
26. Babic A, Lindner AB, Vulic M, Stewart EJ, Radman M (2008) Direct visualization of horizontal gene transfer. *Science* 319(5869):1533–1536.
27. He S, et al. (2015) The IS200/IS605 family and "peel and paste" single-strand transposition mechanism. *Microbiol Spectr*, 10.1128/microbiolspec.MDNA3-0039-2014.
28. Barabas O, et al. (2008) Mechanism of IS200/IS605 family DNA transposases: Activation and transposon-directed target site selection. *Cell* 132(2):208–220.
29. Guynet C, et al. (2008) In vitro reconstitution of a single-stranded transposition mechanism of IS608. *Mol Cell* 29(3):302–312.
30. Ton-Hoang B, et al. (2005) Transposition of ISHp608, member of an unusual family of bacterial insertion sequences. *EMBO J* 24(18):3325–3338.
31. He S, et al. (2011) Reconstitution of a functional IS608 single-strand transpososome: Role of non-canonical base pairing. *Nucleic Acids Res* 39(19):8503–8512.
32. He S, et al. (2013) IS200/IS605 family single-strand transposition: Mechanism of IS608 strand transfer. *Nucleic Acids Res* 41(5):3302–3313.
33. Lutz R, Bujard H (1997) Independent and tight regulation of transcriptional units in *Escherichia coli* via the LacR/O, the TetR/O and AraC/I1-I2 regulatory elements. *Nucleic Acids Res* 25(6):1203–1210.
34. Calos MP, Miller JH (1981) The DNA sequence change resulting from the IQ1 mutation, which greatly increases promoter strength. *Mol Gen Genet* 183(3):559–560.
35. Markwardt ML, et al. (2011) An improved cerulean fluorescent protein with enhanced brightness and reduced reversible photoswitching. *PLoS One* 6(3):e17896.
36. Nagai T, et al. (2002) A variant of yellow fluorescent protein with fast and efficient maturation for cell-biological applications. *Nat Biotechnol* 20(1):87–90.
37. Shaner NC, et al. (2004) Improved monomeric red, orange and yellow fluorescent proteins derived from Discosoma sp. red fluorescent protein. *Nat Biotechnol* 22(12):1567–1572.
38. Kinney JB, Murugan A, Callan CG, Jr, Cox EC (2010) Using deep sequencing to characterize the biophysical mechanism of a transcriptional regulatory sequence. *Proc Natl Acad Sci USA* 107(20):9158–9163.
39. Bire S, et al. (2013) Transposase concentration controls transposition activity: Myth or reality? *Gene* 530(2):165–171.
40. Landgraf D, Okumus B, Chien P, Baker TA, Paulsson J (2012) Segregation of molecules at cell division reveals native protein localization. *Nat Methods* 9(5):480–482.
41. Kuhlman TE, Cox EC (2012) Gene location and DNA density determine transcription factor distributions in *Escherichia coli*. *Mol Syst Biol* 8:610.
42. Nayak CR, Rutenberg AD (2011) Quantification of fluorophore copy number from intrinsic fluctuations during fluorescence photobleaching. *Biophys J* 101(9):2284–2293.
43. Kuhlman TE, Cox EC (2013) DNA-binding-protein inhomogeneity in *E. coli* modeled as biphasic facilitated diffusion. *Phys Rev E Stat Nonlin Soft Matter Phys* 88(2):022701.
44. Luria SE, Delbrück M (1943) Mutations of bacteria from virus sensitivity to virus resistance. *Genetics* 28(6):491–511.
45. Kessler DA, Levine H (2013) Large population solution of the stochastic Luria-Delbruck evolution model. *Proc Natl Acad Sci USA* 110(29):11682–11687.
46. Ha T (2014) Single-molecule methods leap ahead. *Nat Methods* 11(10):1015–1018.
47. Galas DJ, Chandler M (1982) Structure and stability of Tn9-mediated cointegrates. Evidence for two pathways of transposition. *J Mol Biol* 154(2):245–272.
48. Scott M, Gunderson CW, Mateescu EM, Zhang Z, Hwa T (2010) Interdependence of cell growth and gene expression: Origins and consequences. *Science* 330(6007):1099–1102.
49. Acharya S, Foster PL, Brooks P, Fishel R (2003) The coordinated functions of the *E. coli* MutS and MutL proteins in mismatch repair. *Mol Cell* 12(1):233–246.
50. Kuhlman TE, Cox EC (2010) Site-specific chromosomal integration of large synthetic constructs. *Nucleic Acids Res* 38(6):e92.
51. Kuhlman TE, Cox EC (2010) A place for everything: Chromosomal integration of large constructs. *Bioeng Bugs* 1(4):296–299.
52. del Solar G, Giraldo R, Ruiz-Echevarría MJ, Espinosa M, Díaz-Orejas R (1998) Replication and control of circular bacterial plasmids. *Microbiol Mol Biol Rev* 62(2):434–464.
53. Tucker WT, Miller CA, Cohen SN (1984) Structural and functional analysis of the par region of the pSC 10 1 plasmid. *Cell* 38(1):191–201.
54. Gaglia G, Guan Y, Shah JV, Lahav G (2013) Activation and control of p53 tetramerization in individual living cells. *Proc Natl Acad Sci USA* 110(38):15497–15501.
55. Tas H, Nguyen CT, Patel R, Kim NH, Kuhlman TE (2015) An integrated system for precise genome modification in *Escherichia coli*. *PLoS One* 10(9):e0136963.
56. Goñi-Moreno A, Amos M, de la Cruz F (2013) Multicellular computing using conjugation for wiring. *PLoS One* 8(6):e65986.
57. Goñi-Moreno A, Amos M (2012) Discrete modelling of bacterial conjugation dynamics. arXiv:1211.1146.
58. Kuhlman T, Zhang Z, Saier MH, Jr., Hwa T (2007) Combinatorial transcriptional control of the lactose operon of *Escherichia coli*. *Proc Natl Acad Sci USA* 104(14):6043–6048.

SYSTEMS BIOLOGY